



<https://doi.org/10.30678/fjt.146786>

© 2024 The Authors

Open access (CC BY 4.0)

## An innovative evaluation of microstructure and tribological behavior of AISI 1060 and CuZn37Pb2 under laboratory and complex working conditions

M. Seyf Eddine Bougoffa<sup>1</sup>, Sayhia Benchaa<sup>2</sup>, Hadibi Abdelhak<sup>1</sup>, Benmesbah Ouissem<sup>3</sup>, Benkhaled Sihem<sup>3</sup>, Labiod Yasmine<sup>3</sup>

<sup>1</sup>Laboratory of Advanced Technologies in Mechanical Production, Department of Mechanical Engineering, University of Badji Mokhtar, Laboratory LMI, Annaba, Algeria

<sup>2</sup>Laboratoire de Rayonnement et Plasmas et Physique des Surfaces (LRPPS), Faculté des Mathématiques et des Sciences de la Matière, Université de Ouargla, 30000 Ouargla, Algeria

<sup>3</sup>Laboratory Networks and Systems Laboratory-LRS, Department of computer science, University of Badji Mokhtar, P.o.Box 12, Annaba. 23000, Algeria

Corresponding author: M. Seyf Eddine Bougoffa (mohamed-seyf-eddine.bougoffa@univ-annaba.dz)

### ABSTRACT

Wear is a significant industrial issue caused by the interaction of multiple complex factors rather than solely by material properties. CuZn37Pb2 and AISI 1060 steel are particularly susceptible to wear due to extensive industrial applications. This study developed a wear test tool, machined on a horizontal lathe, for testing under dry and lubricated conditions. A tribological comparison was conducted between the lathe test and a tribometer, examining factors like surface roughness, load, sliding speed, wear track diameter, track width, contact temperature, wear loss, and wear rate relative to the friction coefficient. Experiments were performed with torques ranging from 25 to 100 N, speeds of 0.30, 0.40, and 0.50 m/s, and wear track diameters of 4, 6, 8, and 10 mm. Worn surfaces and wear tracks were analyzed using optical microscopy and SEM-EDS. The influence of temperature (50 °C to 200 °C) on friction properties was studied, showing that sample morphology and test type greatly affect tribological response. Despite a wear rate calculation error below 8.12%, results indicated differences between laboratory and real-world tribological responses. This study enhances wear understanding by examining numerous previously unstudied characteristics and shows that, although wear cannot be entirely eliminated, it can be significantly minimized. Laboratory testing provides prototypes for industrial challenges, effectively linking academic research with industry needs.

**Keywords:** CuZn37Pb2; AISI 1060; Temperature; Wear track diameter; Wear mechanism; Wear debris.

### 1. Introduction

Due to its substantial economic impact, wear has long captivated the interest of researchers. AISI 1060 and CuZn37Pb2 are two materials that are highly sought in industrial applications owing to their unique mechanical, physical, and economic properties [1,2]. Wear is recognized as a phenomenon resulting from the interaction of various interconnected and complex factors, rather than being an inherent material property [3,4]. Given that wear is often detrimental, industry professionals strive to prevent it or to achieve adequate protection against it to mitigate its effects. Consequently, various techniques, including surface treatment, are employed. The effect of flux concentration on the structure and mechanical properties of CuZn37Pb2 was examined, and the optimal flux concentration for enhancing these properties was determined [5]. After subjecting study material [6] to subcritical and full

annealing as well as hardening via quenching and tempering, the authors conclude that the plastic deformation of AISI 1060 steel increases with rolling pressure and number of passes due to increased cold work intensity, and that under comparable deep rolling conditions, fully annealed specimens exhibit more severe deformation than subcritical annealed specimens. Furthermore, when the hardness of the original material increases, the capacity of deep rolling to improve surface hardness diminishes. Deep rolling varied yield and ultimate tensile strength values differently based on the condition of the work material, and deep rolling converted residual tensile stresses measured after rolling into compressive values. Higher rolling pressure and number of passes had distinct effects on the subsurface fine hardness distribution, depending on the state of the work material. Mehdinia [7] conducted an experiment to determine the effects of quenching and heat treatment on AISI 1060 steel's

fatigue behavior, tempering temperature, and hardening time. The samples were initially annealed at 800 °C for one hour before being cooled in a 25 °C water bath. 1 and 2 hours were spent tempering at 250°C, 450°C, and 650°C, respectively. Increasing the setting time and tempering temperature decreased the hardness, tensile strength, and fatigue limit, as indicated by the mechanical properties. The results of scanning electron microscopy (SEM) indicated that crack propagation was slower in samples diluted at 250 °C for 1 h compared to samples at higher temperatures and for a longer time. Increasing the tempering temperature also increased the regions of fatigue crack germination and accelerated crack propagation. S. Senhadji et al. [8] evaluate the frictional and wear behavior of two pins, CuSn9P and CuZn39Pb2, sliding on a steel disc under mixed lubrication (XC42). This study [9] evaluated the effect of friction and disturbing loads on the toughness, tensile properties, and microstructure of welded joints. According to experimental findings, the values for hardness and tensile strength increase with increasing friction and disturbing stresses. On the AISI 1060 side of the welded connection, a tensile fracture developed. Optical and scanning electron microscopy were used to assess the integrity and face quality of the treated friction joints. To achieve perfect interfacial bonding, substantial disturbance loads and friction must be present, as well as excessive plastic deformation to bring these materials into the region of attraction. The objection or criticism directed towards this research is not the limitation of the results it concluded, because there are many limits imposed by the means used in the investigations or imposed by a lack of resources, nor is it the large number of industrial, technical, and economic costs proposed by these researches as a treatment to reduce wear and tear, but rather what is taken on these research is primarily based on this approach. This study assumes that prior literature was like someone who rushed to fix an issue without giving it the time it deserved to be understood and analyzed, and it did not receive an accurate diagnosis. Only a few studies followed this path, particularly those that focused on these topics [10-12]. One of these studies that undertook an analytical study of wear was conducted by Tefvik Küçükömeroğlu and LeventKara [10]. The sliding friction and wear behavior of CuZn39Pb3 were examined using an environmentally controlled pin-on-disk system under both air and vacuum conditions. The CuZn39Pb3 alloy's wear mechanism was primarily adhesive in both atmospheric and vacuum conditions; however, considerable abrasion was seen under atmospheric conditions. Under vacuum circumstances, the wear rate of the CuZn39Pb3 was reduced. Furthermore, raising the applied pressure increased the wear of the alloy substantially under atmospheric conditions but only modestly under an 810-6 mbar vacuum. The alloy tested in air showed extensive subsurface deformation.

Understanding wear and its associated variables is neither straightforward nor trivial, necessitating careful attention and detailed investigation. This study posits that

by focusing efforts on understanding this complex phenomenon—characterized by numerous interacting variables—and by analyzing the interactions between these variables while minimizing the influence of some pre-controlled or reducible variables, it may be possible to achieve better predictions and outcomes. The comparative case study presented in this paper exemplifies the importance of studying wear and evaluating its characteristics, on par with research aimed at addressing wear issues. CuZn37Pb2 and AISI 1060 steel, due to their extensive industrial applications, are among the materials most susceptible to wear. To contribute to solving this problem and to enrich the scientific literature, an initial step should involve understanding and analyzing the impact of all these interrelated factors and their interactions through comprehensive experimental investigations. This study developed a novel wear test apparatus, machined on a horizontal lathe, to perform tests under both dry and lubricated conditions. A tribological comparison was made between the lathe test and the tribometer, considering the interaction of multiple factors. Variables such as initial surface roughness, load, sliding speed, and track width, along with contact temperature, wear loss, and wear rate, were investigated and compared to the friction coefficient. Experiments were conducted at torques ranging from 25 to 100 N, speeds of 0.30, 0.40, and 0.50 m/s, and wear track diameters of 4, 6, 8, and 10 mm. The worn surfaces and wear tracks of each sample were examined using optical microscopy, XRD patterns, and SEM-EDS.

Understanding wear and its associated variables is neither straightforward nor trivial, necessitating careful attention and detailed investigation. This study posits that by focusing efforts on understanding this complex phenomenon - characterized by numerous interacting variables—and by analyzing the interactions between these variables while minimizing the influence of certain controllable variables, it may be possible to achieve better predictions and outcomes. The comparative case study presented in this paper exemplifies the importance of studying wear and evaluating its characteristics, which is equally important as research aimed at addressing wear issues. CuZn37Pb2 and AISI 1060 steel, due to their extensive industrial applications, are among the materials most susceptible to wear. To contribute to solving this problem and to enrich the scientific literature, an initial step should involve understanding and analyzing the impact of all these interrelated factors and their interactions through comprehensive experimental investigations. This study developed a novel wear test apparatus, machined on a horizontal lathe, to perform tests under both dry and lubricated conditions. A tribological comparison was made between the lathe test and the tribometer, considering the interaction of multiple factors. Variables such as initial surface roughness, load, sliding speed, track width, contact temperature, wear loss, and wear rate were investigated and compared to the friction coefficient. Experiments were conducted at torques

ranging from 25 to 100 N, speeds of 0.30, 0.40, and 0.50 m/s, and wear track diameters of 4, 6, 8, and 10 mm. The worn surfaces and wear tracks of each sample were examined using optical microscopy, XRD patterns, and SEM-EDS.

## 2. Experimental Method

It is not easy to study tribological behavior in which numerous entangled elements interact. Despite all of the study that has been published, the literature still requires further research and experimental studies on this topic. Most crucially, they require publications that connect academic research to industrial reality. Many studies on this topic have been written in order to bridge the gap between laboratory experiments and the industrial field [13-15]. However, most of them are always partial and do not cover all elements of the issue, maybe due to the vastness of this field and the impossibility to satisfy all of the intervening circumstances. Because it is nearly impossible to perform an empirical examination that addresses all of the components that contribute to the conventional phenomenon, most research concentrates on particular factors while neglecting or ignoring others. There are studies that particularly address the effect of surface roughness on tribological behavior [16-18], studies that deal with tribological Behavior under dry and lubricated conditions [19-21], and research that deal with friction under different geometrics [22-25]. Furthermore, there are very few studies that deal with the study of the effect of these various tribological factors on materials in their raw state [26-28], the study of the tribological behavior of materials to which reinforcements have been added is not always a positive trend, this research deals with a comparative tribology study that takes into account all of the aforementioned factors, in addition to studying the contact temperature under high temperatures.

The study's limitations are due to technical difficulties, such as the inability to compare the pin-on-disc test and the ball-on-disc test under lubricated conditions, the inability to study the measurement of contact temperature in a ball-on-disc test, and the inability to study the coefficient of friction in the pin-on-disc test.

### 2.1. Laboratory Trials

The purpose of this experiment is to investigate the frictional and wear characteristics of CuZn37Pb2 and SAE-AISI 1060 with varying wear track diameter and surface roughness of samples. Wear tests were carried out on a tribometer (CSM Instruments, model TRB3) with a specific load range and speed settings to analyze friction and wear characteristics at a temperature of 20 °C. Since the performance of CuZn37Pb2 and SAE-AISI 1060 was critical to the findings of this experimental investigation, and due to the many parameters influencing the results of the tribological behavior, the wear track was designed so that every point was subjected to different operating condition. The significance of utilizing distinct wear tracks is to determine the difference between CuZn37Pb2 and SAE-AISI 1060's coefficient of friction (Figure 1).

The tests vary three parameters:

#### 1. Speed (V [m/s])

$$V = \pi DN / 60 * 1000$$

$D = 2r$  (r being the distance between the centre of the pin and the axis of rotation of the sample) and which is varied by 6mm, 8mm and 10 mm

N: Rotation speed (on the tribometer we will choose the speed:  $V = 955$  [rpm])

So:

$$V_1 = \pi DN / 60 * 1000 = \pi * 6 * 955 / 60 * 1000 = 0.30 \text{ m/s}$$

$$V_2 = \pi DN / 60 * 1000 = \pi * 8 * 955 / 60 * 1000 = 0.40 \text{ m/s}$$

$$V_3 = \pi DN / 60 * 1000 = \pi * 10 * 955 / 60 * 1000 = 0.50 \text{ m/s}$$

The variation in speed will affect the distance travelled (L) such that:  $L = \pi D N t$

Duration of the test for each sample:  $t = 30$ min

#### 2. The distance traveled (d[m])

$$D_1 = V_1 * t = 540 \text{ m}$$

$$D_2 = V_2 * t = 720 \text{ m}$$

$$D_3 = V_3 * t = 900 \text{ m}$$

#### 3. The applied force (Fn [N])

Which will have the following values: 25N, 50N, 75N, 100N, each force will be applied to all the samples (which is subjected to 3 rotational speeds).

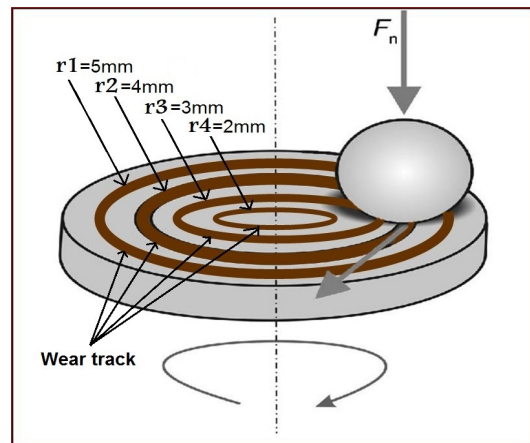


Fig. 1. Pin-on-disc test setup.

### 2.2 History of service

Very few experimental investigations have relied on the lathe test to study tribological behavior [29-31]. Moreover, according to the authors there is a few tribological study that compared a lab test with a test device. The frictional process between the pin and the disc is continuously subjected to the normal force thanks to the system's installation on the turret of a horizontal universal lathe. This is accomplished as a result of a function that is based on the idea of a lever at a left angle that is activated by a force causing a couple on a pin leaning on a revolving surface. The force (F) that is applied to the remote arm (a) by masses that are placed on the arm is then amplified and applied in a direction that is perpendicular to the arm. This

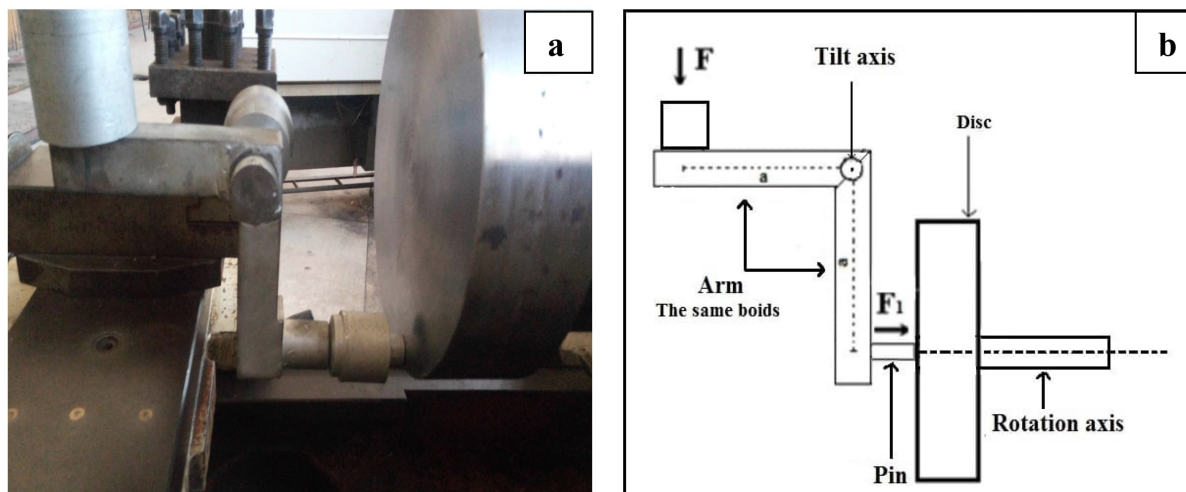


Fig. 2. (a) Illustration of (a) a pin-on-disc wear device and (b) an experimental test.

force is then applied to the pin that is in direct contact with the surface of the disc that is installed on the lathe chuck. When the pin and the disc are moving past one another while being rotated, a surface wear track is produced that has the appearance of a circular track as a result of the sliding contact between the pin and the disc and the effect of the application force. A sample with oblique edges was used so that there would be real contact between the specimen and the disc and so that there would not be wear on the side edges of the sample.

$$\sum M / 0 = 0$$

$$F \times a + F_1 \times a = 0$$

$$F = -F_1$$

We isolate the system: So:  $-F_1 = F_1 \implies F = F_1$

For reasons of convenience of materials and dimensions of the samples, we have chosen the following features:

There is 147mm between the pin's hub and the disc's rotational axis.

The length of the arm is 210 millimetres. The pin is 15 mm in diameter.

### 2.3 Used Materials

A cylinder samples (Table 1) of CuZn37Pb2 and AISI 1060 (diameter 15 mm, length 25 mm) were chosen to be used as disc materials in Tribometer tests. CuZn37Pb2 and AISI 1060 are often used in some heavy duty industrial applications that require materials with better machinability. Some of these applications are mentioned: Aerospace applications (i.e. helicopter rotor skins), Truck frames Rail coaches, Motorboats, Boiler-making, Rivets, Ship building operations, Tube exercise equipment, Military and commercial bridges, Transport operations, Towers and pylons. Most of these various industrial applications are subject to friction and wear, which requires studying the impact of these applications (addressing the largest possible number of interfering factors) on the structural, mechanical and tribological properties of the samples [32,33]. Balls of 100Cr6 Steel with a diameter of 6 mm is placed in contact with a known and

regulated speed and vertical load on the surface of the samples. Extremely high mechanical performance is typically required for the kinds of applications [34-36] where 100Cr6 Steel is used. In the other hand, a disc of 100Cr6 Steel with a 240 mm diameter was used in the test device. While dry and lubricated conditions in the test device were prepared on AISI 1060 and CuZn37Pb2 samples. The initial roughness and hardness of samples, discs, and balls used in the study are listed in Table 1.




### 2.4 Protocol for Experiments

The sample's wear loss that happened during testing is regarded as an evolving wear parameter as a function of time. The volume loss was calculated using the density of CuZn37Pb2, which is 8.44 g/cm<sup>3</sup> (VL). AISI 1060 weighs 7.85 g/cm<sup>3</sup> and has a density of 7.85 g/cm<sup>3</sup>. The wear rate (WR) of the specimens was calculated using the volume loss (VL) and sliding distance (SD) values.

The base units of measurement for sliding distance (SD) and volume loss (VL) are both meters (cm<sup>3</sup>). The contact temperature was measured using a UNI-T IR thermometer, model UT 301C. This gadget can measure temperatures ranging from -18 to 550 degrees Celsius. A pin-on-disc wear test was performed with the contact continually immersed in lubricant bath maintained using lubricant neutral 100  $\eta = 0.034$  Pa.s.

All specimens had their surface roughness measured before and after the wear test. Surface roughness was measured in several directions based on the sliding direction. Imaging and surface analysis were conducted using an SEM (FEI Quanta 450) with a high accelerating voltage kV to observe microstructural changes. For initial surface roughness assessment, we employed an optical microscope (Olympus BX53) with a high magnification to capture high-resolution images. Table 2 contains full information on each test's parameters (tribometer and test device).

**Table 1.** Materials tested in summary

Specimen	Material	Hardness	Ra	Photos	
Samples	CuZn37Pb2	170±0.5 HB	0.32-0.97-1.44 µm	 Before test	 After Lab test  After Test device
	AISI 1060	183±0.5 HB	0.91-1.69-2.30 µm	 Before test	 After Lab test  After Test device
Ball	100Cr6 Steel	780 HV30	0.09 µm	 Before test	 After Lab test
Disc		780 HV30	0.1 µm	 Before test	 After Test device

### 3. Results and Discussion

#### 3.1 Microscopic Observations

The AISI 1060 and CuZn37Pb2 alloys were chosen as the work materials. Their applications range from railroad components to landing gears to stamping tools, dies, and

punches. The SEM micrographs of AISI 1060 steel (Fig. 3.a) show the presence of iron particulates. The SEM micrographs of CuZn37Pb2 (Fig. 3.b) clearly show the presence of two phases (Figure 3.b):  $\alpha$  consisting of clear dendrites rich in copper and  $\beta$  which appears in dark brown. The black spots observed in the photograph represent lead.

**Table 2.** Parameter breakdown for the pin-on-disc.

N°	Limits	Tribometer	Test device
1	Speed of motor	955 tr/min	90;65;50 tr/min
2	The distance between the disc's centre and its axis of rotation.	10;8;6;4 mm	107;115;118mm
3	Surface condition	Dry	Dry-Lubricated
4	Duration	1800 s	
5	Speed	0.50;0.40;0.30 m/s	
6	Distance	900;720;540 m	
7	Temperature	20(±0.1) °C	
8	Load	100;75;50;25 N	

The brass used is of type CuZn37Pb2, which contains 37% zinc and 2% lead. From the Cu-Zn phase diagram (Figure 3.b), this type of brass is two-phase in nature. An  $\alpha$  phase which is a solution of zinc in copper, rich in copper and of a face-centred cubic (FCC) structure. A second phase  $\beta$ , corresponding to the matrix, has a higher zinc content with a centred cubic lattice. This last phase occurs at high temperatures and is characterized by a disordered distribution of atoms. At temperatures below 454~468°C, the arrangement of copper and zinc atoms in this phase becomes ordered and the  $\beta$  phase is then denoted  $\beta'$ . This one is harder and more fragile. Lead particles can be observed in the phases and more particularly at the interface of the  $\alpha/\beta$  phases. The  $\alpha$  phase is characterized by good ductility and aptitude for cold deformation, while the  $\beta$  phase is hard and brittle, thus increasing the hardness of the material and promoting chip splitting. Various studies have shown that most of the physical properties of brasses are influenced by the zinc content. The addition of lead (up to 3%), unlike other addition elements, practically does not modify the properties of brass. Lead is soluble in molten brass but precipitates at grain boundaries during

solidification, generating particles ranging in size from 1 to 10  $\mu\text{m}$ . [37,38]. It thus promotes the fragmentation of chips during machining. In addition, it acts as a lubricant due to its low melting point, as indicated in the work of N. Gane [39] for dry sliding friction, where the coefficient of friction increased from 0.62 for a brass ( $\alpha/\beta$ ) without lead at 0.32 with lead. In fact, lead forms a discontinuous phase throughout the material and allows the reduction of the COF between the part and the tool, and consequently reduces their wear.

### 3.2 Frictional behavior

The frictional behavior was studied in four ways. The first was the friction coefficient under varying beginning roughness, temperature, lubricated state, wear track diameters, and contact temperature.

#### 3.2.1 Initial Roughness Compared to the Friction Coefficient

Figure 4 show how the average friction coefficient of CuZn37Pb2 and AISI 1060 evolves over time based on the

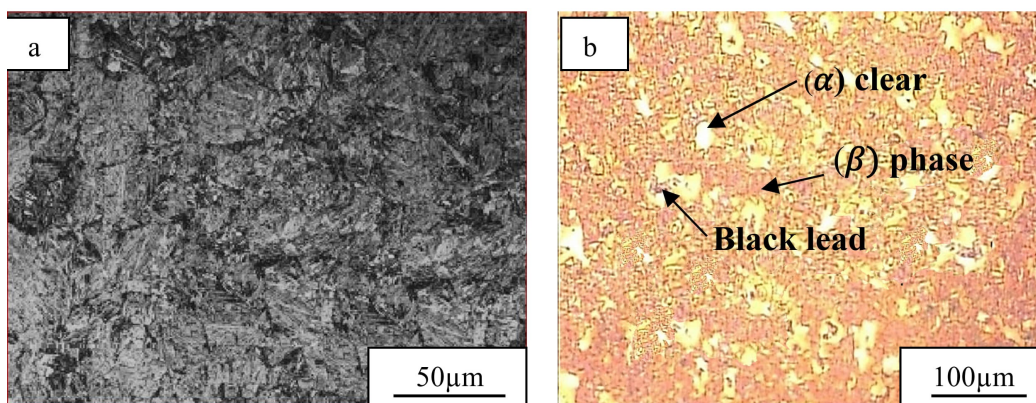


**Fig. 3.** The microstructures of a) AISI 1060 steel and b) CuZn37Pb2

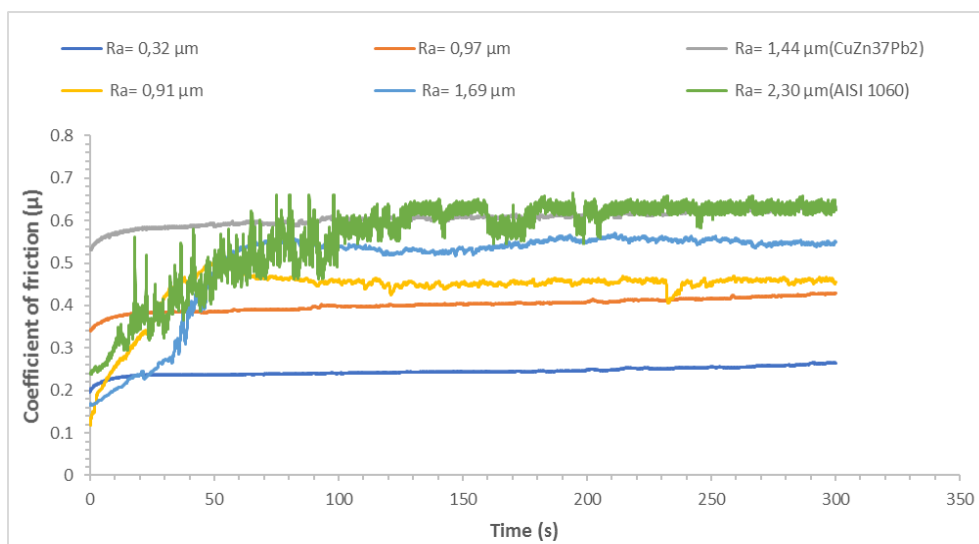


**Fig. 4.** Time dependence of the frictional coefficient between CUZN37PB2 and AISI 1060 at various levels of initial roughness ( $F=50\text{N}$  ;  $V=0,40\text{m/s}$ ).

beginning roughness. These wear tests were performed with a 50 N load and a sliding velocity of 0.35 m/s. The initial roughness of the sample appears to have some influence on the frictional characteristics of CuZn37Pb2, according to the findings. It is worth noting that the surface roughness of CuZn37Pb2 ( $R_a = 1.44\ \mu\text{m}$ ) produced the highest coefficient of friction (0.58), but the surface roughness of AISI 1060 ( $R_a = 2.30\ \mu\text{m}$ ) produced the highest coefficient of friction (0.60). The consequences of initial roughness are more pronounced for AISI 1060 COF (0.60). Surface roughness increases the friction coefficient, according to these figures. This causes the industry and its applications to avoid using samples with rough surfaces as much as possible, especially when using AISI 1060. This is owing to the fact that the friction process begins with a wide contact area, which then expands due to sliding wear, resulting in a greater friction coefficient. Previous research [15-18] and their findings on the coefficient of friction are congruent.

### 3.2.2 Friction Coefficient under elevated temperature

It is necessary to have a better understanding in the influence of rising temperature on coefficient friction. The influence of temperature on friction Coefficient of CuZn37Pb2 and AISI 1060 are shown in Figures 5,6. When the temperature increases from 50 to 200 °C at  $F=50\text{N}$  ;  $V=0,40\text{m/s}$ , the coefficient of friction increases from 0.47 to 0.57 for AISI 1060; when the temperature increases from 50 to 200 °C at  $F=50\text{N}$ ;  $V=0,40\text{m/s}$ , the coefficient of friction increases from 0.24 to 0.39 for CuZn37Pb2. The results demonstrate that temperature has a significant impact on friction properties [40-42]. As the contact pressure increases, the coefficient of friction tends to decrease. This tendency appears to be lessened as the tool temperature rises. According to the author, as mentioned by Merklein et al. [43], the change in tribological behavior results from the alteration in lubricant viscosity caused by the temperature

increase on the tool surfaces.

### 3.2.3 Friction Coefficient versus Load and Wear Track Diameters

The coefficient of friction of CuZn37Pb2 and AISI 1060 under various normal loads is shown in Figure 7 (A), as measured by testing on a 6 mm worn track. The friction coefficient of CuZn37Pb2 decreases from 0.39 at 25N to 0.28 at 100N, according to the results. Sliding on the surfaces is likely to occur in the interval immediately following the start of the transition. The creation of debris, also known as the third lab test, causes a considerable decline in COF during the wear process, which continues until the condition stabilizes. AISI 1060, on the other hand, rises from 0.50 at 25N to 0.59 at 100N. As the load increases, the friction coefficient of AISI 1060 increases. This increase in friction coefficient can be attributed to the sample's enhanced adhesion strength to the pin as a result of the increased stress. In identical conditions, it indicates that CuZn37Pb2 has much less friction than AISI 1060.

Figure 7 (B) depicts the coefficient of friction of CuZn37Pb2 and AISI 1060 during dry sliding wear at various wear track diameters. The results shown that employing concentric wear tracks of varying widths produces consistent surface friction and wear outcomes [44,45]. The fact that the findings were obtained demonstrated this. There is minimal difference in the coefficient of friction curves of CuZn37Pb2 and AISI 1060, and there is no relationship between the difference in coefficient of friction and track wear diameters, according to evidence.

### 3.2.4 Relationship of the Contact Temperature and the Friction Coefficient to the Load and the Speed

Figures 8 (a, b) depict the tribometer-measured coefficient of friction (Lab test) as well as the test bench-measured contact surface temperature (Lath test) of

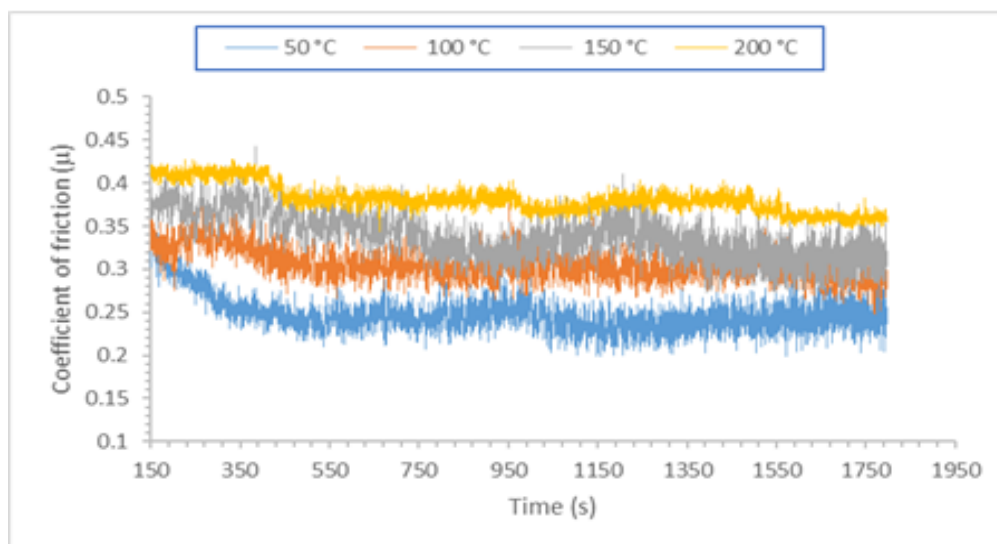


Fig. 5. Frictional coefficient of CuZn37Pb2 under lubricated condition ( $F=50\text{N}$  ;  $V=0,40\text{m/s}$ ).

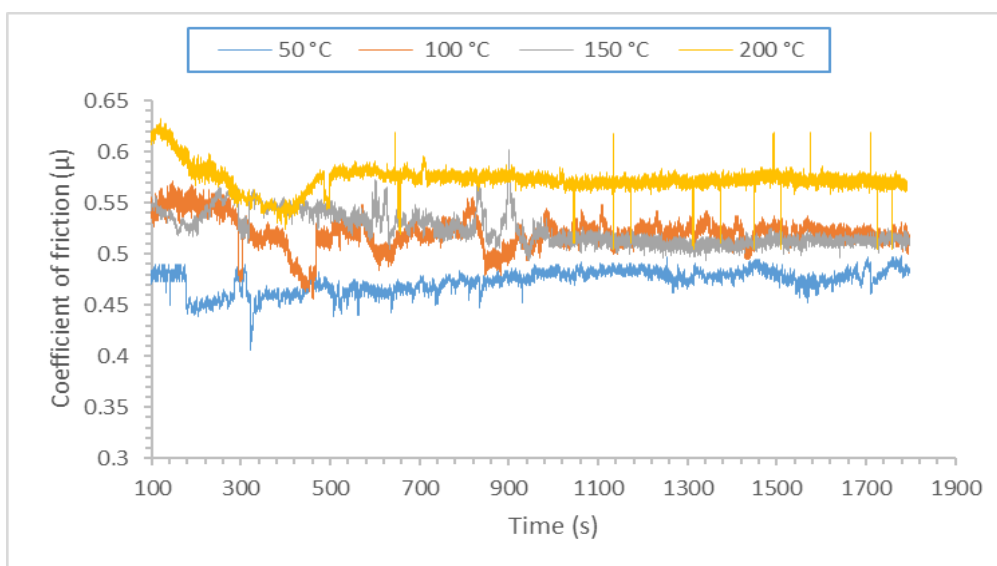
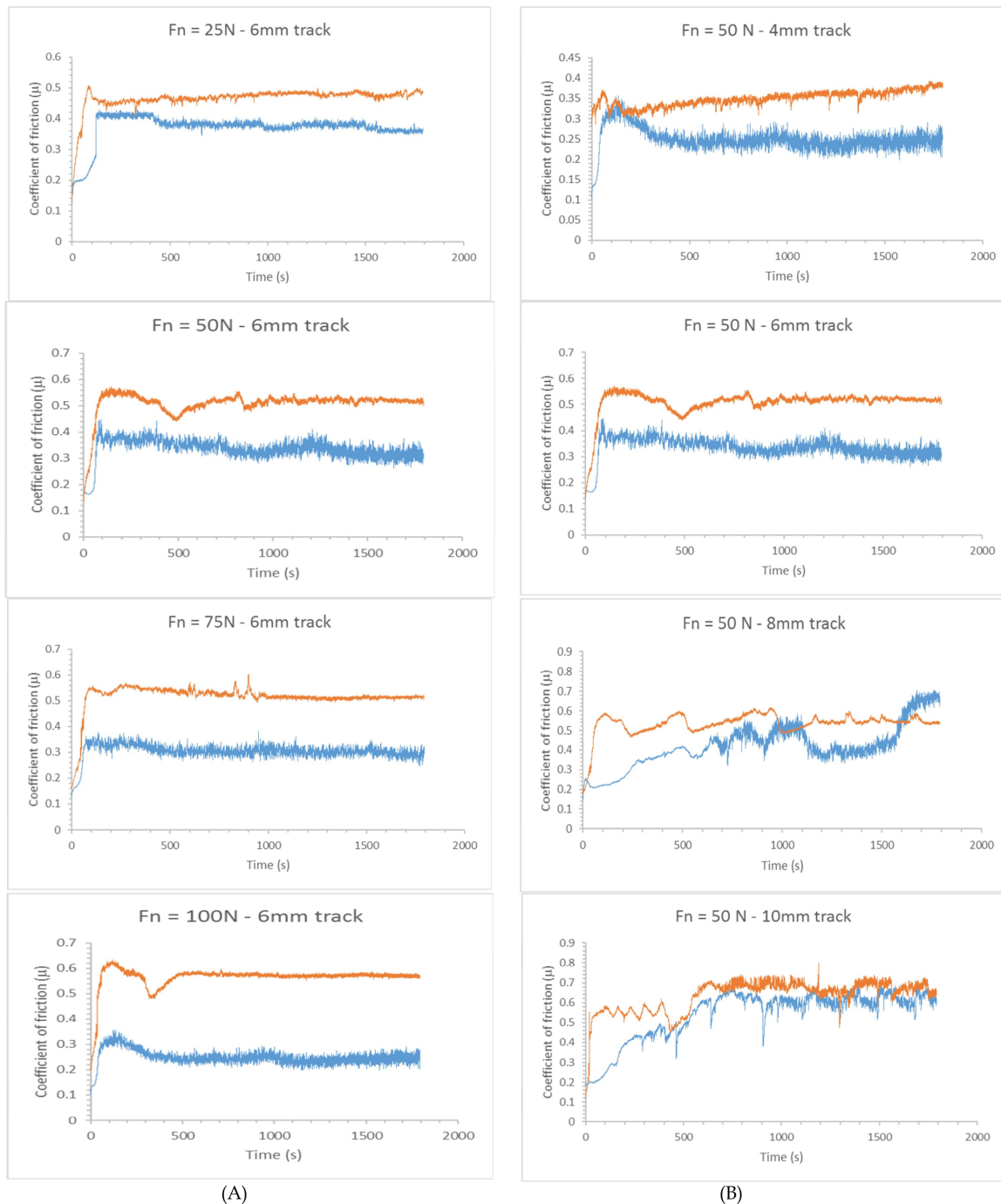


Fig. 6. Frictional coefficient of AISI 1060 under lubricated condition ( $F=50\text{N}$  ;  $V=0,40\text{m/s}$ ).

CuZn37Pb2 and AISI 1060. When the normal load was increased from 50 N to 100 N at a sliding speed of 0.30 m/s, the results showed that the COF for CuZn37Pb2 changed from 0.40 to 0.34. This occurred when the sliding speed was maintained at 0.30 m/s. Coefficient of friction was found to range from 0.40 at a velocity of 0.30 m/s to 0.25 at a velocity of 0.40 m/s, according to the measurements that were taken. The manner in which the force is transferred from the pin to the disc shifts depending on the type of wear test, which results in a frictional coefficient that shifts in response to changes in load and velocity. Because the asperities of the antagonists become entangled and imbricated with one another under low stresses, adhesion between surfaces that are in contact with one another is typically improved. Plastic deformations become more significant as the tangential force increases. Oxidation of surfaces, which results in the formation of an oxide layer that acts as a lubricant, is promoted by the heat created by mechanical friction and the increasing surface temperature

of contact. Another thing that helps with sliding is that the particles separate from the CuZn37Pb2 and move to the counter face. The patterns observed in these data are in agreement with those discovered in the research [17]. The decrease in the COF of CuZn37Pb2 that occurs when the sliding speed increases could be attributed to variations in shear rate. When the normal load is increased from 50 to 100 N at a sliding speed of 0.40 m/s, the COF for AISI 1060 shifts from 0.51 to 0.54. This shift could be caused by an increase in adhesion strength. The results of this investigation are consistent with earlier research [18]. The COF for AISI 1060 was calculated to be 0.52 at a speed of 0.30 m/s and 0.54 at a speed of 0.40 m/s. The COF increases in proportion to the increase in velocity. It is feasible to explain that the heat created at the asperities reduces the strength of the specimen, resulting in a stronger adhesion with the disc. Researchers discovered equivalent results; thus, this conclusion is compatible with the findings of those researchers [19]. On the other hand,





**Fig. 7.** AISI 1060 and CuZn37Pb2 friction coefficient curves under (A) various normal loads tested on a 6mm diameter worn track. The -50 N value was used in Test Condition (B) to simulate varying wear track diameters.

the value of the temperature difference changes from 1.6 °C to 1.8 °C for AISI 1060 when the normal load increases from 50 to 100 Newtons at a sliding speed of 0.30 m/s; for CuZn37Pb2, the value of the temperature difference changes from 0.7 °C to 1.8 °C when the normal load increases from 50 to 100 Newtons at a sliding speed of 0.40 m/s; It should be noted that the initial temperature of iron and brass before conducting the wear experiment is 10.9 °C. Temperature measurements obtained during the wear test (Figures 8 (a, b)) show that the apparent temperature does not change. The Pin on Disc or Ball on Disc test

reveals that the majority of frictional heat flows towards the counter face disk rather than the pin [20-22]. This is evidenced by the fact that the temperature rises just slightly. Both the COF (Lab test) measured by a tribometer and the contact surface temperature (Lath test) measured by a test bench for AISI 1060 and CuZn37Pb2 rise exponentially up to a certain distance, then level off. This demonstrates that the wear mechanisms investigated in both of these studies are comparable to one another and consistent with one another.

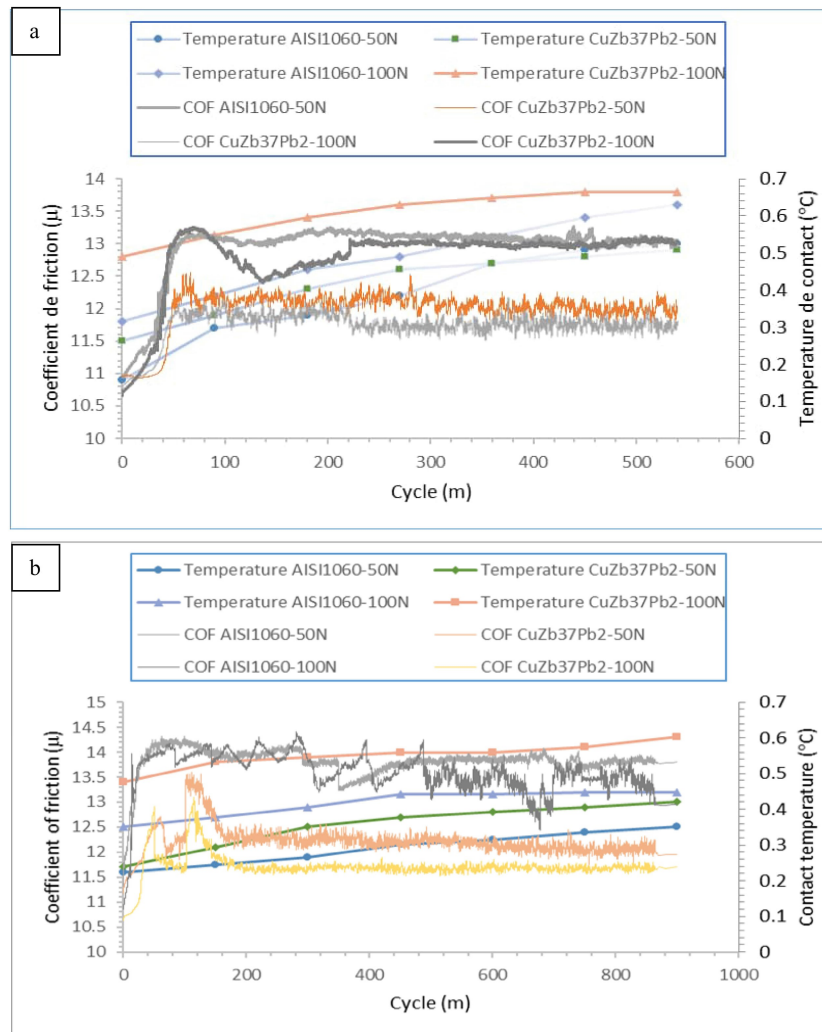


**Fig. 8.** Contact surface temperature (Lath test test) with coefficient of friction obtained in Lab test of CuZn37Pb2 and AISI 1060 at a) 0.30 m/s and b) at 0.40 m/s

### 3.3 Wear behavior

Six characteristics of wear behavior have been investigated. The first one is the study of the correlation between wear loss, track width and friction coefficient, the second aspect is concerned with wear Loss under dry and lubricated condition, the third is based on wear rate calculation in lab and lathe test, in the fourth aspect the worn surface was analyzed, the fifth component of the results presents the observations of the facie of the pin, sixth element includes analysis of wear debris.

#### 3.3.1 Correlation between wear loss, track width and friction coefficient

Figure 9 depicts how the track width of AISI 1060 changes as a function of normal load and sliding speed. According to these numbers, the width of the track depends on the force applied and the velocity at which the object is sliding. According to the numbers, a wider track is required for a given normal load or sliding speed. Sliding speed has a minor effect on the width of the track for towed materials at load 50N, but a much larger effect at load 100N.

Figure 10 depicts the friction coefficient, wear loss, and

track width of CuZn37Pb2 as a function of normal load and sliding speed. When a load is applied and a sliding speed is set, the coefficient of friction, track width, and wear loss change. The results of a variety of wear tests performed at a wide range of weights or sliding speeds indicate that track width increases as wear loss and coefficient of friction rise. The influence of sliding speed on track width is minor at 50N load but becomes significant at 100N load.

#### 3.3.2 Wear Loss in Relation to Speed and Load under dry and lubricated condition

The wear loss of AISI 1060 and CuZn37Pb2 under dry and lubricated condition are shown in Figure 11. The effectiveness of the friction material must be tested consistently [23] for reliable results. Both tests assume the same wear mechanism, but their observed behaviors suggest otherwise. This demonstrates the usefulness of the lathe test results under dry and lubricated condition and supports the inference that the wear behavior observed in dry and lubricated condition follow a different pattern. The findings also show that under high load and fast sliding

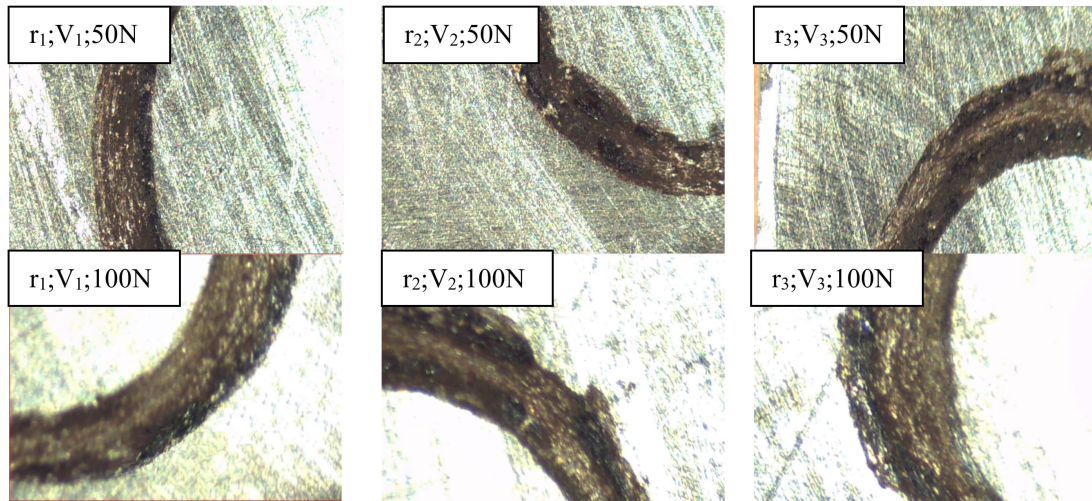


Fig. 9. Optical microscopy of different wear track of AISI 1060

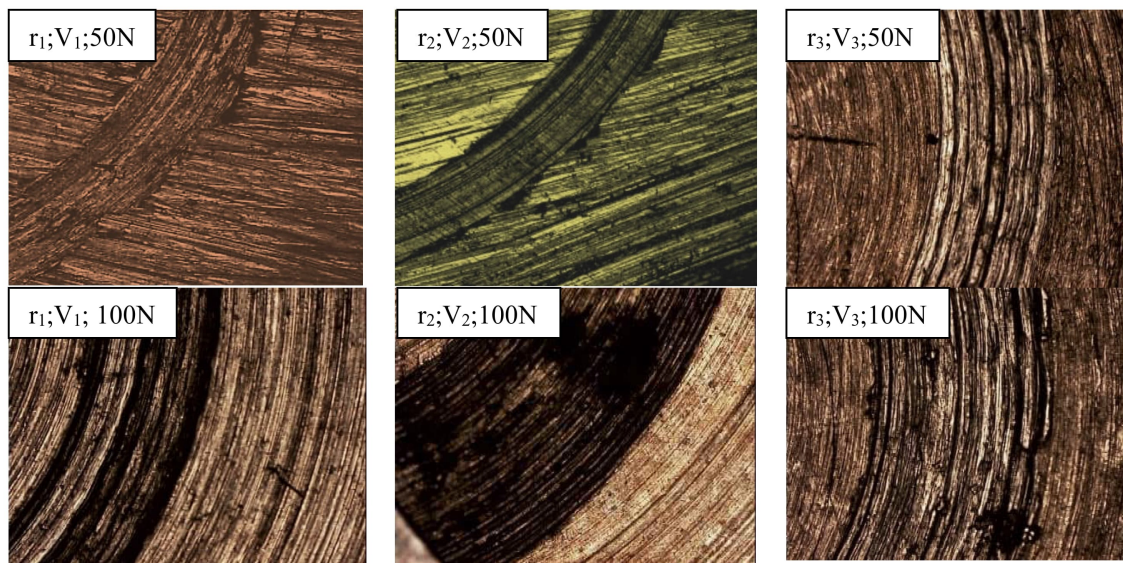


Fig. 10. Optical microscopy of different wear track of CuZn37Pb2

speed, tow alloys wear at a faster rate. When tested with a load of 100N and a sliding speed of 0.50m/s, CuZn37Pb2 and AISI 1060 showed a higher wear loss. The results agree with those found by other scientists [15,46].

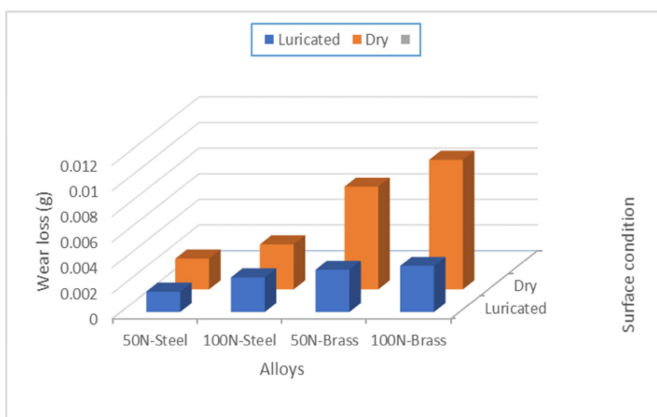
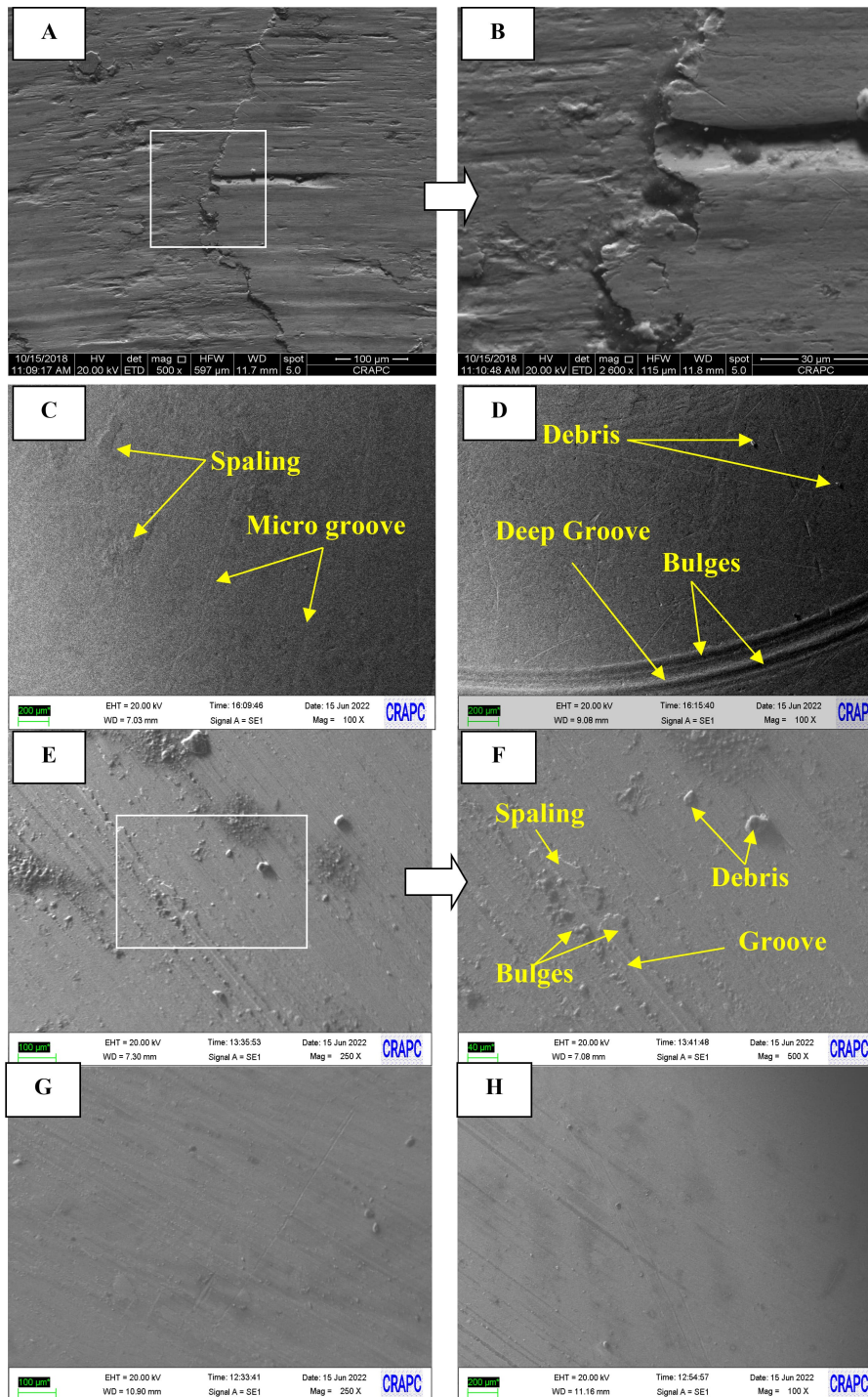


Fig. 11. wear loss of CuZn37Pb2 and AISI 1060 under dry and lubricated condition

Cut lines and grooves on the worn surface and a flake stripping layer in the local structure are shown in Figure 12 (A) for AISI 1060 and Figure 12 (E) for CuZn37Pb2 under dry condition. The worn surfaces of AISI 1060 and CuZn37Pb2 that were noticed in Figure 12 (C, D) and (G, H) respectively, suggests abrasive wear, light spalling wear, and some abrasive wear debris characterize the wear mechanism. It can be clearly distinguished that the wear under dry conditions was severe compared to the wear under lubricated conditions [19-21]. The lubrication of the surfaces in contact facilitates sliding between these surfaces and reduces the shear stresses generated during the test carried out (disappearance of the disturbed zone), consequently, the cracks disappear and  $\mu$  decreases (Fig.12. (c, d)). Wear debris, due to its specific chemical composition, is to blame for the presence of oxides. This can be confirmed in Figures 16,17 obtained. According to experimental evidence, the coefficient of friction is dramatically increased when debris undergoes oxidation due to friction. According to [26], as wear progresses, the coefficient of friction dramatically increases and becomes



(A) and (B) F=50N under dry condition; (C) F=50N and (D) F=100N under lubricated condition; for AISI 1060  
 (E) and (F) F=50N under dry condition; (G) F=50N and (H) F=100N under lubricated condition; for CuZn37Pb2

**Fig. 12.** SEM micrographs of AISI 1060 and CuZn37Pb2 under dry and lubricated condition

relatively high for highly abrasive surfaces. Sliding faster would result in wider and deeper grooves and a larger spalling area. Under 100N load as shown in Figure 12 (D) for AISI 1060 and Figure 12 (H) for CuZn37Pb2, the wear surface undergoes severe plastic deformation. it can be drawn that as load increase, plastic deformation and

material peeling also increase, leading to a rougher worn surface and greater wear loss.

**3.3.3 Wear rate in lab and lathe test**  
 The wear rate of AISI 1060 and CuZn37Pb2 in a lab test and a test device during dry sliding wear are shown in Figure 13. The effectiveness of the friction material must be

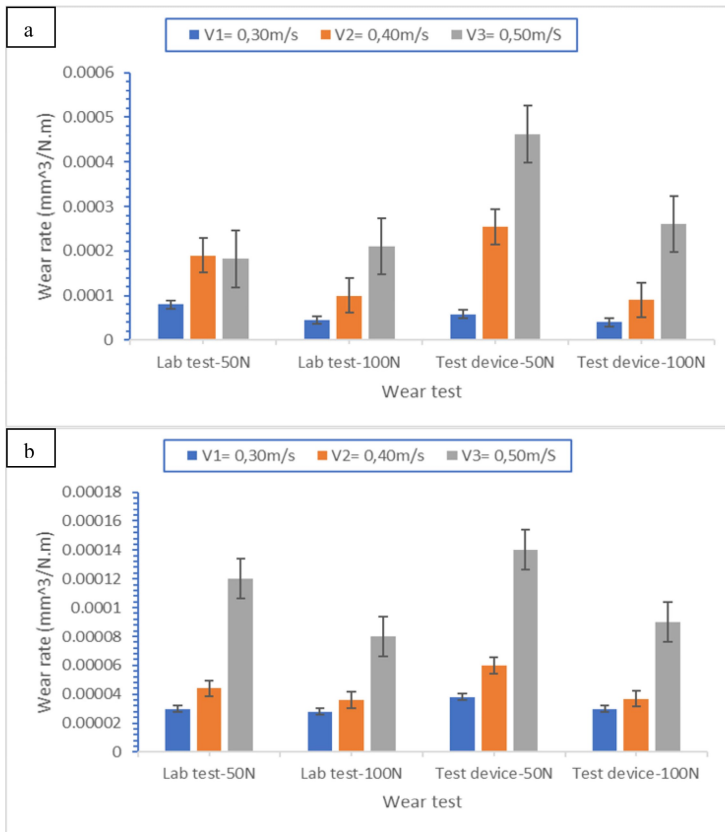


**Fig. 13.** (a) CuZn37Pb2 and (b) AISI 1060 wear rate for tribometer (lab test) and test device (test device)

tested consistently [23] for reliable results. Miniature testing, like the lathe test used in this investigation, is required, however, to speed up production. It can be inferred from the numbers that the curves travel at variable velocities. Both tests assume the same wear mechanism, but their observed behaviors suggest otherwise. This formula was used to determine the percentage of difference in results between the two tests:  $[(W_{r_{Lath\ test}} - W_{r_{Lab\ test}}) / (W_{r_{Lath\ test}} + W_{r_{Lab\ test}})] * 100$ ;  $W_{r_{Lab\ test}}$  is the wear rate from the tribometer and  $W_{r_{Lath\ test}}$  is the wear rate from the lathe. The error deviation rate of CuZn37Pb2 was 4.65 %, 3.42 %, 3.92 %, and 5.14 % at loads: 25, 50, 75, and 100 Newtons, respectively. The error deviation rate of AISI 1060 was 4.98 %, 3.87 %, 5.61 %, and 8.12 % at loads: 25, 50, 75, and 100 Newtons, respectively. According to the error deviation calculator, the difference in wear rate between the two studies is not more than 6.49 %. This demonstrates the usefulness of the lathe test results and supports the inference that the wear behavior observed in lab experiment and test device follow a similar pattern. The findings also show that under high load and fast sliding speed, tow alloys wear at a faster rate. When tested with a load of 100N and a sliding speed of 0.50m/s, CuZn37Pb2 and AISI 1060 showed a higher wear rate. The results agree with those found by other scientists [15,46].

Micrographs of AISI 1060 acquired during a test device and tribometer wear test are shown in. Figures 14 and 15 clearly show the influence of pin geometry on the worn surface. It is also discovered that the worn debris at the straight cylindrical pin is greater than that at the ball, which can be related to the hardness of the alloy surface. These findings show that many characteristics such as pin shape, load, rotational speed, and travel speed have a substantial impact on wear rate. Ploughing grooves and an overall widening of the track in response to load are tell-tale signs of intense abrasive wear. In tribometer wear test, oxidative wear on the contacting surface and abrasive wear as the major wear mechanism cause delamination and bulges. Similar results were also found in another study [24]. Deterioration rate measurements already back this up. The development of grooves in the direction of sliding is another notable feature. These are brought on by the antagonist's (the ball) protrusions and the flow of wear debris. Figure 14 (b) shows that the scratches appear deeper (for the sample used in the tribometer) but are actually more superficial and cover a larger area of contact (for the sample used on the test device). On a larger scale, we notice that the surface contact (the device used to conduct the tests) does not exhibit the same degree of repeatability across trials. The spring in the pin holder is what allows this study's test device to have a slightly higher vibration rate than the previous study's [15]. In addition, we note the presence of cracks along the contact surface of the pin were created (Fig. 14.a) given the severe operating conditions, and the cyclic stresses exerted on the surface. These cracks cause fatigue wear which generates medium-sized active debris at the interface. This debris accumulates and sinks into the pin, tearing the metal (abrasive wear). There is an action of the oxides due to the increase in temperature during the plastic deformation, as confirmed in Figure 14 (b) of the spectra of the dry-tested pion. In addition, there was a transfer of material from the ball to the tracks in contact with the sample during the test Fig. 14(a).

Micrographs of CuZn37Pb2 obtained in two separate experiments (lab test and lath test) are shown in Figure 15. The material is compacted by the ball's movement, in Figure 15 (b) and its movement is facilitated by the material's formation into beads. However, when effort or speed are low, material tends to pass below the ball. For CuZn37Pb2, this is demonstrated with high confidence. However, the lubricating oxide coatings can be eliminated by increasing the normal load. The surface may still be protected by loose particles, but their effect will be much weaker than the oxide layer. The actual contact surface is the sharp edges of the opposing lab testies. Faster and more significant asperity deformation occurs in the tribometer. In fact, as the contact pressure increases, the contact quality also improves: where low loads produce a contact/friction between the roughness, high loads produce perfect friction. Wear is found to occur via abrasive, adhesive, and oxidative mechanisms, with plastic

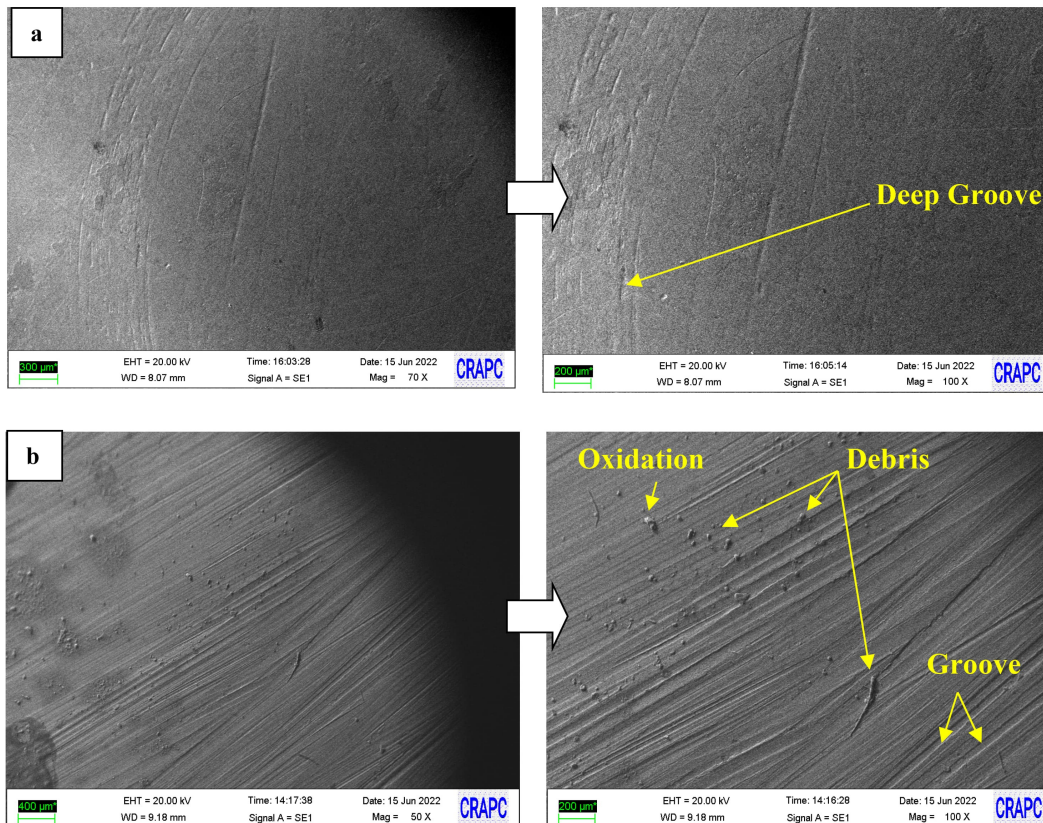


Fig. 14. SEM micrographs of AISI 1060 for (a) tribometer (lab test) and (b) test device (lath test).

deformation and spalling as a corollary. The findings of [15] largely corroborate these results, adding weight to them. Wear on CuZn37Pb2 is much greater than that on AISI 1060.

### 3.3.4 Worn surface analysis

EDS micrograph of AISI 1060 and CuZn37Pb2 spectrum are presented in Figures 16, 17 respectively. EDS analysis

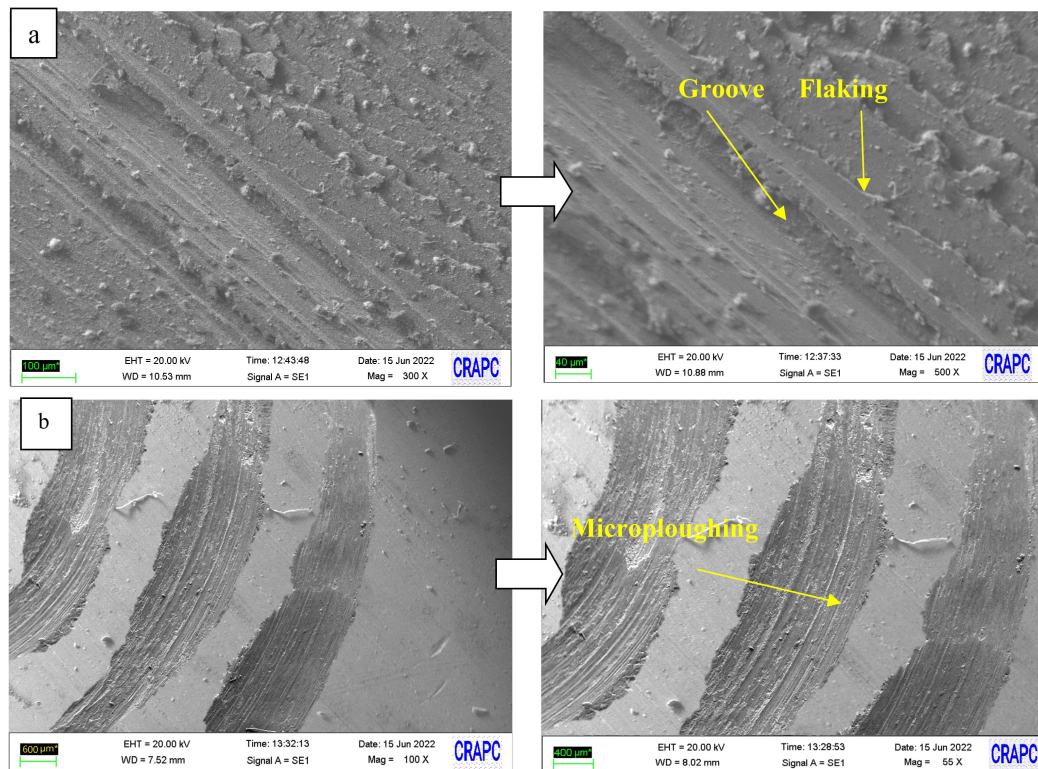


Fig. 15. SEM micrographs of CuZn37Pb2 for (a) test device (lath test) and (b) tribometer (lab test).

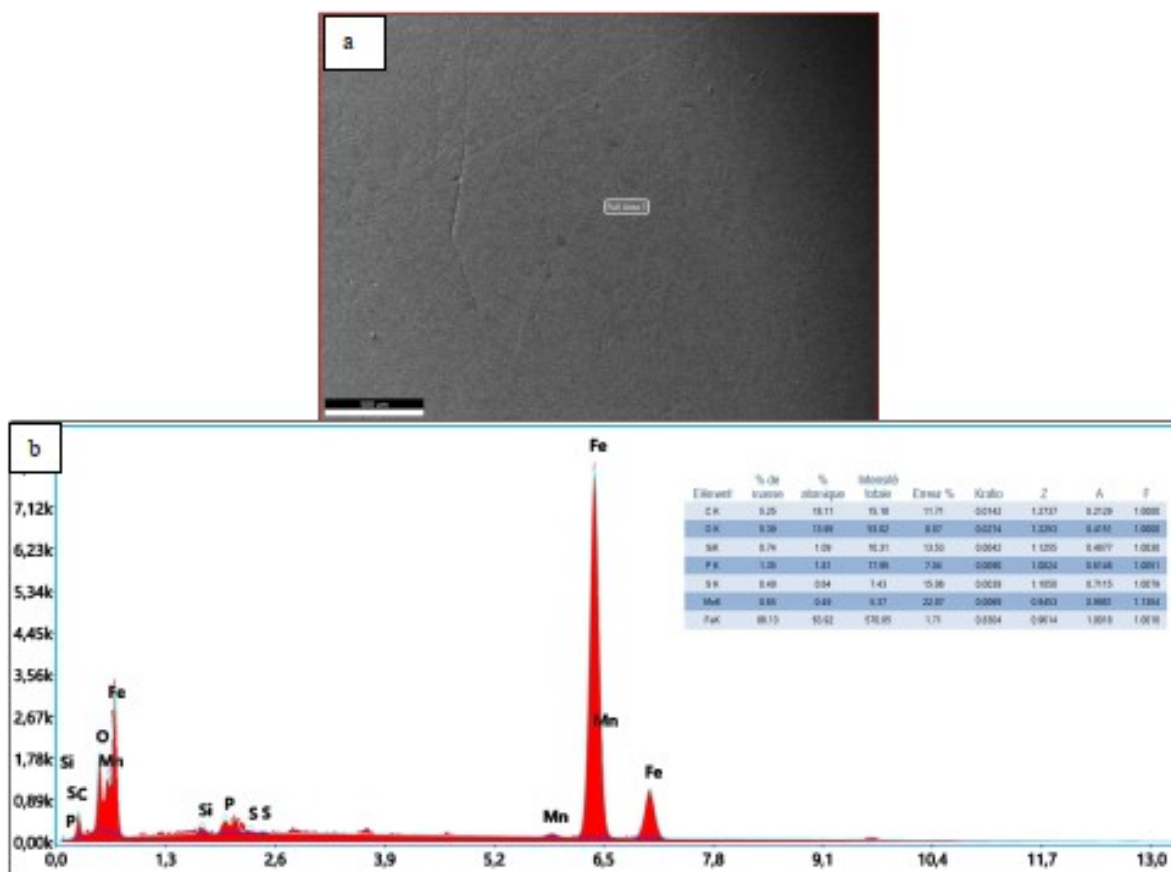


Fig. 16. AISI 1060 EDS spectrum after lath test

confirms the presence of metal in wear track. The elements observed in wear track during the EDS was: 18.11% at. C,

13.95% at. O, 63.92% at. Fe and low contents of other elements. Its average chemical composition is given as

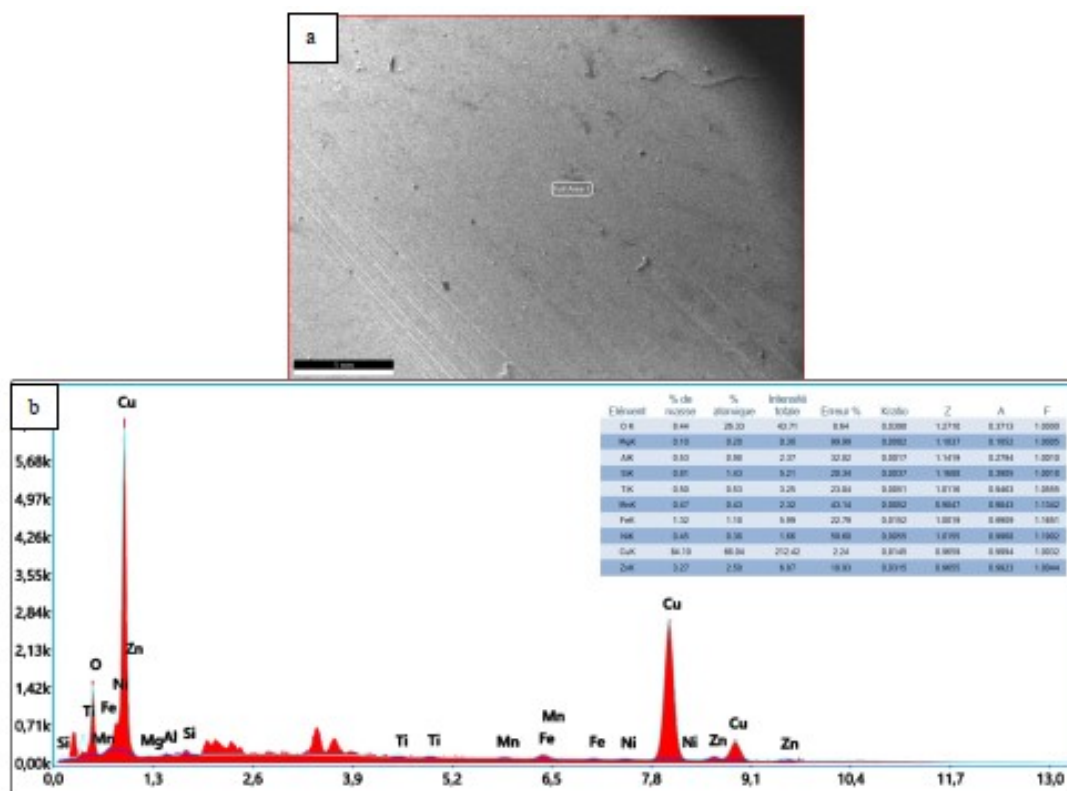
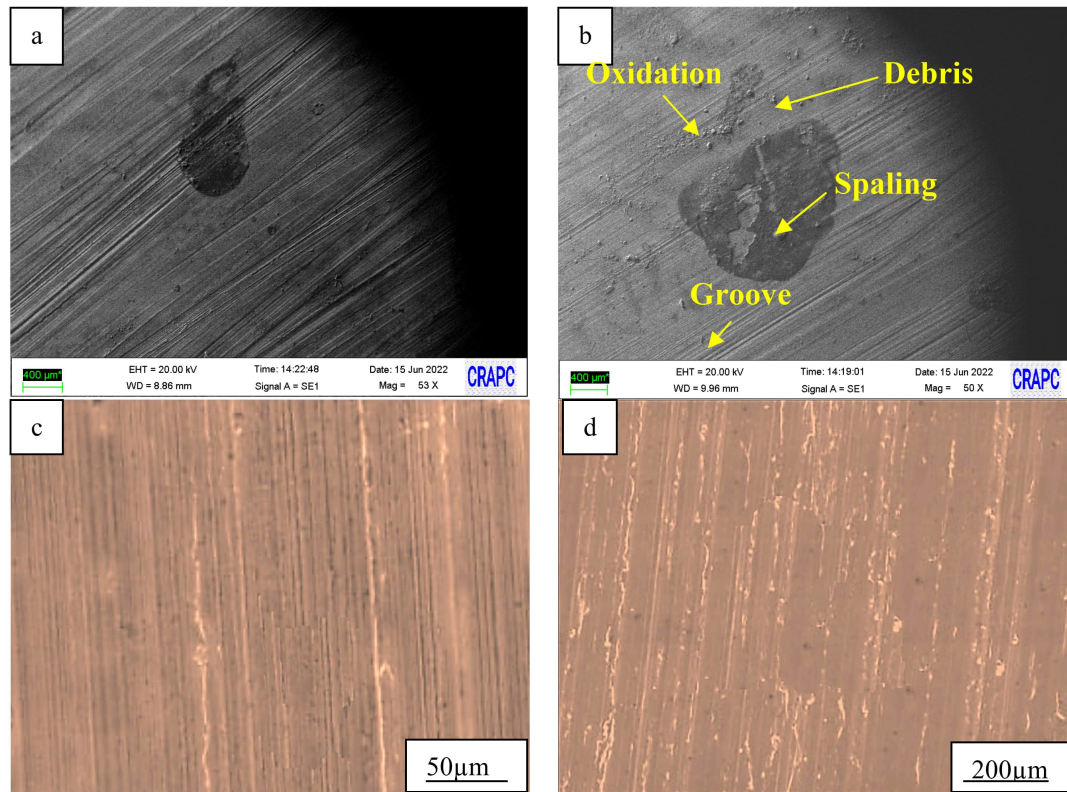


Fig. 17. CuZn37Pb2 EDS spectrum after lab test



(a) 100Cr6 Steel Pin / AISI 1060 Steel smooth, (b) 100Cr6 Steel Pin / AISI 1060 Steel rough, (c) 100Cr6 Steel Pin / CuZn37Pb2 smooth, (d) 100Cr6 Steel Pin / CuZn37Pb2 rough

**Fig. 18.** Facies of the pins after wear test

follows: (1.09%at. Si, 1.81%at. P, 0.64%at. S, 0.49%at. Mn). Mapping analysis showed that the concentration of iron and oxygen is higher than comes the carbon concentration at a lower rate. This indicates the formation of significantly iron enriched transfer layer (Fig. 16). Quantitative EDX spectra obtained from different locations of wear track indicated in the table in inset of Fig 16(b) also showed the higher intensity of iron and oxygen. On the other hand, Mapping analysis of CuZn37Pb2 (Figure 17) showed that the concentration of iron and oxygen is higher than comes the carbon concentration at a lower rate. The elements observed in wear track during the EDS was: 66.04% at. Cu, 2.50%at. Zn, 1.43%at. Si, 1.18%at. Fe, 0.38%at. Ni, 0.43%at.

Mn). This indicates the formation of significantly brass enriched transfer layer (Fig. 17). This surface has experienced four major wear mechanisms: adhesion, abrasion, oxidation and subsequent adhesion wear, and plastic deformation of the cutting edge. Several of the mechanisms can be active at the same time, according to the discussions and supporting micrographs [47-53].

### 3.3.5 Observations of the facie of the pin

Observation under an optical microscope of the wear surfaces of the pins, at the end of the test, shows the formation of ploughed furrows in the direction of sliding (Figure 18). These are due to the roughness of the

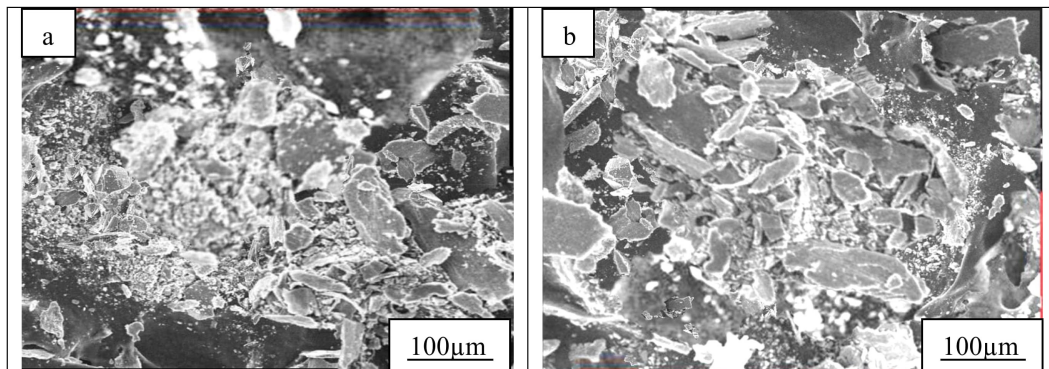


**Fig. 19.** SEM image of the wear debris of 100Cr6 Steel Disc / AISI 1060 Steel smooth, (b) 100Cr6 Steel Disc / AISI 1060 Steel rough



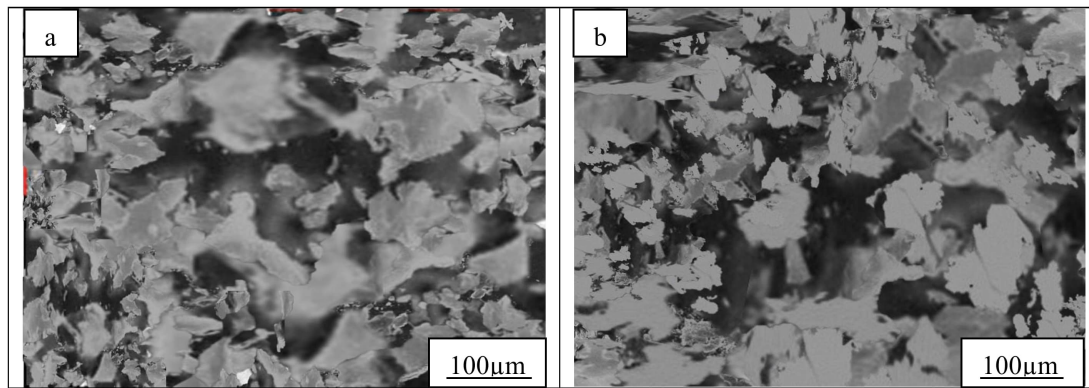


Fig. 20. SEM image of the wear debris of 100Cr6 Steel Disc / CuZn37Pb2 smooth, (b) 100Cr6 Steel Disc / CuZn37Pb2 rough

antagonist (the 100Cr6 Steel disc) and the movement of wear debris. Optical images show that CuZn37Pb2 suffered more severe wear than AISI 1060 Steel. The presence of streaks and wear debris on the facies observed, for the two study materials, allows us to see that the type of wear that occurs during friction is abrasive wear.

### 3.3.6 A study of wear debris

Fig. 19 shows the SEM micrographs of the wear debris of 100Cr6 Steel Disc / AISI 1060 Steel sample as a function of roughness. The wear debris generated during the wear tests is recovered by filtering the oil and is analyzed by scanning electron microscopy. This analysis shows that the shape and quantity of iron debris depends on the roughness of the disc. They are flattened with rough outlines for the smooth disc (Figure 19(a)), and elongated and small in size for the rough disc (Figure 19(b)). Part of the debris generated is transferred to the disc. It is indicated by a trace visible to the naked eye. Clearly visible is a shift in the size and form of the wear debris as the surface roughness increases. At a lower roughness, more equiaxed and less flake-shaped wear debris is formed. Debris of a small size suggests that the wear rate was lower with lower surface roughness. The quantity of flake-shaped particles increases as surface roughness increases. At a greater roughness, larger-sized debris are evident. This discovery shows that more material was lost at a faster rate, which decreased the wear resistance at increasing surface roughness.

Despite the limitations of this method, it cannot be overlooked that there are some insufficient results, so the results indicate that the small amount of debris generated during wear of AISI 1060 Steel is primarily due to these high mechanical properties (elastic limit, breaking strength, etc.) that provide it with good rigidity [54]. It is hypothesized that the pressure exerted causes the tops of the asperities to flatten, reducing the roughness of the surface and explaining the minimal amount of debris.

The amount of debris recovered from the 100Cr6 Steel / CuZn37Pb2 couple is very small, with a random flat shape (Figure 20: a and b). The wear trace on the disc, for its part, is almost weakly detectable (Figure 20). This indicates that for the same test conditions, AISI 1060 Steel offers better

adhesive wear resistance compared to CuZn37Pb2.

## 4. Discussion

The aim of this research was to deepen the understanding of wear phenomena, influenced by a complex interplay of factors. The interaction among these wear factors was investigated and analyzed using available experimental methodologies. This study particularly focused on microscopic observations of AISI 1060 and CuZn37Pb2 alloys. The author's attention was directed not only towards frictional behavior, including initial roughness compared to the friction coefficient; the impact of temperature (between 50°C and 100°C) on frictional properties; friction coefficient variation with load and wear track dimensions; and the relationship between contact temperature, friction coefficient, load, and speed, but also on wear behavior, encompassing correlations between wear loss, track width, and friction coefficient; wear loss under dry and lubricated conditions relative to speed and load; wear rate comparisons between laboratory and lathe tests; analysis of worn surfaces; observations of pin facies; and examination of wear debris. When comparing AISI 1060 and CuZn37Pb2 (Figure 4), it was observed that the initial surface roughness of AISI 1060 exerted a greater influence on its coefficient of friction (COF). Comparison of previous tests using equipment based on the compression spring principle [15,46] versus the lever principle revealed a slight increase in vibration rate during the friction process. While CuZn37Pb2's COF decreases during friction, AISI 1060's COF increases with normal load, sliding speed, and contact surface temperature, significantly surpassing that of CuZn37Pb2 (Figure 5, 6). With increased load or sliding speed, the temperature of the contact surface, frictional thrust, and shear force all escalate, accelerating the wear process. Wear loss is closely linked to track width, with track width being more directly influenced by load than speed (Figure 7). The study results clearly demonstrated that initial surface roughness correlates with transition stress and wear loss during the shift from high to low wear conditions. Regarding friction, as surfaces slide against each other, the temperature of the sliding surfaces gradually rises, leading to thermal softening and eventual plastic flow, thereby increasing the actual contact area. The real contact between the test

sample surfaces and the disk (illustrated in Figure 7) causes the friction coefficient to rise over time, although after approximately 150 seconds, the contacting surfaces continue to slide, stabilizing the friction coefficient to its steady-state value. Experimental findings also indicated that the coefficient of friction for brass is lower at lower loads compared to higher loads (Figure 7, 8). When substantial loads are applied, the true contact area between the sample surface and the disk expands due to plastic deformation of surface protrusions over time. The increase in friction coefficient for AISI 1060 with increasing applied stress is attributed to the enlargement of the real contact area between the test sample and the disk surfaces. The wear mechanism observed in the samples (Figures 16, 17) is linked to increased plastic deformation of surface protrusions under higher loads, resulting in higher dislocation density, hardness, and material fragility as microcracks form due to dislocation accumulation. These cracks propagate under applied forces, converging at weak spots and generating significant fissures. Upon contact with each other or with wear lines, these fissures dislocate thin layers of metal, which are then removed in the direction of sliding motion, forming wear debris particles. Upon comprehensive literature review, methodological gaps were identified, highlighting the need for diverse research methods to generate new insights or mitigate biases. The originality of our method and findings lies in addressing this gap. The data obtained broadly align with major trends in the field [55]. Though limitations exist, primarily stemming from the unavailability of experimental tools and analysis resources, potential applications of these findings are commonly discussed in the concluding section.

## 5. Conclusion

This study aims to compare the findings of wear tests conducted with the newly developed device to those obtained from standard laboratory wear tests using a CSM tribometer. Tribological parameters were examined for both pin-on-disc and ball-on-disc contact types for CuZn37Pb2 and AISI 1060 alloys, considering the effects of initial surface roughness, stress, and sliding speed. The key conclusions of this research are as follows:

1. When comparing AISI 1060 and CuZn37Pb2, AISI 1060's initial surface roughness has a more significant impact on its coefficient of friction (COF). During the friction process, CuZn37Pb2's COF decreases, whereas AISI 1060's COF increases with normal load, sliding speed, and contact surface temperature, and is substantially higher than that of CuZn37Pb2.

2. Temperature (ranging from 50 °C to 200 °C) has a profound effect on the friction characteristics of the two alloys. As the load or sliding speed increases, the temperature of the contact surface, frictional thrust, and shear force all rise, thereby accelerating the wear process. The test results clearly demonstrated that initial surface roughness correlates with transition stress and wear loss

during the shift from high to low wear.

3. There is a consistent correlation between wear loss and track width, with track width being more closely related to load than to speed. When comparing a test device based on the compression spring principle to one based on the lever principle, a slight increase in vibration rate was observed during the friction process with the latter.

4. Under identical working conditions, both the lathe test and the lab test show similar wear mechanisms. The error deviation in wear loss calculations does not exceed 8.12% in either test. However, optimal laboratory conditions cannot be directly transferred to real-world working environments.

This study underscores the need to introduce an analysis of surface states, a recent development aimed at providing an experimental depiction of this poorly understood phenomenon.

## Nomenclature

COF: coefficient of friction

## Conflict of Interest

The authors declare that they have no conflict of interest.

## Funding

There is no funding source.

## Ethical approval

This article does not contain any studies with human participants or animals performed by any of the authors.

## References

- [1] Amir Alsammarrarie et al (2020) Studying the tribological behavior of the Counterface Materials 60/40 Brass alloy under Dry Sliding Contact. IOP Conf. Series: Materials Science and Engineering 870. <https://doi.org/10.1088/1757-899X/870/1/012151>
- [2] Serkan Islak, Soner Buytoz, Muzaffer Karagöz (2012) Microstructural development on AISI 1060 steel by FeW/B4C composite coating produced by using tungsten inert gas (TIG) process. Indian Journal of Engineering & Materials Sciences 19 : 253-259. <http://hdl.handle.net/11772/5171>
- [3] Cheng Zhang et al (2019) Effect of Tempering Temperature on Impact Wear Behavior of 30Cr3Mo2WNi Hot-Working Die Steel. Front. Mater. 6:149. <https://doi.org/10.3389/fmats.2019.00149>
- [4] M Bartoszuk, BMS Eddine (2021) Numerical modelling of heat dissipation for the Pin-On-Disc type tribometer. International Journal for Engineering Modelling 34 : 19-30. <https://hrcak.srce.hr/file/367205>

- [5] Mariusz Jenek1, Paweł Schlafka (2021) An influence of slag refining on the structure and mechanical properties of the brass CuZn39Pb2. *The International Journal of Advanced Manufacturing Technology* 117:2519–2525. <https://doi.org/10.1007/s00170-021-07321-x>
- [6] A.M. Abrão et al (2014) The influence of heat treatment and deep rolling on the mechanical properties and integrity of AISI 1060 steel. *Journal of Materials Processing Technology* 214 : 3020–3030. <https://doi.org/10.1016/j.jmatprotec.2014.07.013>
- [7] M. Mehdiinia, S. A. Jenabali Jahromi (2015) Effect of Heat Treatment Process on the Fatigue Behavior of AISI 1060 Steel, *International Journal of ISSI* 12 : 28-32. <https://docplayer.net/26607867-Effect-of-heat-treatment-process-on-the-fatigue-behavior-of-aisi-1060-steel.html>
- [8] Milentije Lukovic (2019) The Influence of Surface Temperature on the Coefficient of Static Friction. *The Physics Teacher* 57: 636. <https://doi.org/10.1119/1.5135798>
- [9] [H. Ates, N. Kaya (2014) Mechanical and microstructural properties of friction welded AISI 304 stainless steel to AISI 1060 steel. *archives of metallurgy and materials* 59:841–846. <https://doi.org/10.2478/amm-2014-0142>
- [10] Tevfik Küçükömeroğlu, Levent Kara (2014) The friction and wear properties of CuZn39Pb3 alloys under atmospheric and vacuum conditions. *Wear* 309:21–28. <http://dx.doi.org/10.1016/j.wear.2013.10.003>
- [11] F. A. P. Fernandes et al (2013) Wear Evaluation of Pack Boronized AISI 1060 Steel. *Materials Performance and Characterization* 2 : 58–66. <https://doi.org/10.1520/MPC20120009>
- [12] Maleki, E., Farrahi, G.H., Reza Kashyzadeh, K. et al. Effects of Conventional and Severe Shot Peening on Residual Stress and Fatigue Strength of Steel AISI 1060 and Residual Stress Relaxation Due to Fatigue Loading: Experimental and Numerical Simulation. *Met. Mater. Int.* 27 (2021) 2575–2591. <https://doi.org/10.1007/s12540-020-00890-8>
- [13] Singh J, Chatha SS, Sidhu BS, Abrasive wear behavior of newly developed weld overlaid tillage tools in laboratory and in actual field conditions. *J Manuf Process* 55 (2020) 143–152. <https://doi.org/10.1016/j.jmapro.2020.03.040>
- [14] Valtonen K, Ratia V, Ojala N, Kuokkala V-T (2017) Comparison of laboratory wear test results with the in-service performance of cutting edges of loader buckets, *Wear*. 388–389 : 93–100. <https://doi.org/10.1016/j.wear.2017.06.005>
- [15] BOUGOFFA. M. Seyf Eddine, Bachirbey M. Nabil, Benouali Chahrazed, T. Sayah, Mamoun Fellah, Mohammed Abdul Samad (2021) Dry Sliding Friction and Wear Behavior of CuZn39Pb2 and AA7075 Under Industrial and Laboratory Conditions. *J Bio Tribo Corros* 7 : 38. <https://doi.org/10.1007/s40735-021-00475-x>
- [16] Kubiak KJ, Liskiewicz TW, Mathia TG (2011) Surface morphology in engineering applications: influence of roughness on sliding and wear in dry fretting. *Tribol Int.* 44 : 1427–1432. <https://doi.org/10.1016/j.triboint.2011.04.020>
- [17] Pradeep L, Menezes K, Satish VK (2009) Influence of roughness parameters and surface texture on friction during sliding of pure lead over 080 M40 steel. *Int J Adv Manuf Technol* 43 : 731–743. <https://doi.org/10.1007/s00170-008-1756-2>
- [18] Senhadji S, Belarifi F, Robbe-Valloire F (2016) Experimental investigation of friction coefficient and wear rate of brass and bronze under lubrication conditions. *Tribol Ind* 38 : 102–107. <https://www.tribology.rs/journals/2016/2016-1/11.pdf>
- [19] I.L. Singer, S. Fayeulle, P.D. Ehni (1996) Wear behavior of triode-sputtered MoS<sub>2</sub> coatings in dry sliding contact with steel and ceramics. *Wear* 195:7–20. [https://doi.org/10.1016/0043-1648\(95\)06661-6](https://doi.org/10.1016/0043-1648(95)06661-6)
- [20] Samiul Kaiser, M. S. Kaiser (2020) Wear Behavior of Commercial Pure Copper with Al and Zn under Dry, Wet and Corrosive Environment, *J. Mater. Environ. Sci* 11 : 551-563. [https://www.jmaterenvironsci.com/Document/vol11/vol11\\_N4/JMES-2020-1149-Kaiser.pdf](https://www.jmaterenvironsci.com/Document/vol11/vol11_N4/JMES-2020-1149-Kaiser.pdf)
- [21] Recep Demirsöz (2022) Wear Behavior of Bronze vs. 100Cr6 Friction Pairs under Different Lubrication Conditions for Bearing Applications. *Lubricants*. 10 : 212. <https://doi.org/10.3390/lubricants10090212>
- [22] Shiv Pratap Singh Yadav et al (2022) Effect of Pin Geometry and Orientation on Friction and Wear Behavior of Nickel-Coated EN8 Steel Pin and Al6061 Alloy Disc Pair, *Advances in Materials Science and Engineering*. 3274672. <https://doi.org/10.1155/2022/3274672>
- [23] Argatov I and Chai YS (2020) Contact Geometry Adaptation in Fretting Wear: A Constructive Review. *Front. Mech. Eng* 6. <https://doi.org/10.3389/fmech.2020.00051>
- [24] S. Mezlini (2006) Effect of indenter geometry and relationship between abrasive wear and hardness in early stage of repetitive sliding, *Wear*. 260 : 412–421. <https://doi.org/10.1016/j.wear.2005.02.106>
- [25] Tanmaya Mishra, Matthijn de Rooij, Dirk J. Schipper (2021) The effect of asperity geometry on the wear behavior in sliding of an elliptical asperity. *Wear* 470–471 :203615. <https://doi.org/10.1016/>

- [j.wear.2021.203615](https://doi.org/10.1016/j.wear.2021.203615)
- [26] Jourani A, Bouvier S (2015) Friction and wear mechanisms of 316L stainless steel in dry sliding contact: effect of abrasive particle size. *Tribol Trans* 58 :131–139. <https://doi.org/10.1080/10402004.2014.955229>
- [27] Autay R, Kchaou M, Elleuch K, Dammak F (2013) Tribological behavior of carbon and low alloy steels: effect of mechanical properties and test conditions. *Tribol Mater Surf Interfaces* 5 :133–140. <https://doi.org/10.1179/1751584X11Y.0000000022>
- [28] Lyu Y, Wahlström J, Tu M, Olofsson U, Friction A (2018) Wear and emission tribometer study of non-asbestos organic pins sliding against AISiC MMC Discs. *Tribol Ind* 40 : 274–282. <https://doi.org/10.24874/TI.2018.40.02.11>
- [29] Oлару S-C et al (2017) Investigation of the sound intensity level in the case of a universal lathe. *MATEC Web Conf* 112 : 6. <https://doi.org/10.1051/matec-conf/201711201025>
- [30] Tabacaru LL, Axinte E, Musca G (2016) Experimental research on the elastic deformation mode of S235JR rolled steel fastened between the centers of a Universal Lathe. *Mater Sci Eng* 161 : 012050. <https://doi.org/10.1088/1757-899X/161/1/012050>
- [31] Junaidi SH, Ahmad Y, Jumadi E (2017) Implementation analysis of cutting tool carbide with cast iron material S45 C on universal lathe. *J Phys: Conf Ser* 930 : 012044. <https://doi.org/10.1088/1742-6596/930/1/012044>
- [32] Krishna, Karthik.M (2014) Evaluation of Hardness Strength of Aluminium Alloy (CuZn37Pb2) Reinforced With Silicon Carbide. *International Journal on Recent Technologies in Mechanical and Electrical Engineering (IJRMEE)* 1 : 014–018. <https://www.semanticscholar.org/paper/Evaluation-of-Hardness-Strength-of-Aluminium-Alloy/6d553bad950c9ba30435423e0abdec3535719c9a>
- [33] Mia, M., Dhar, N.R (2019) Prediction and optimization by using SVR, RSM and GA in hard turning of tempered AISI 1060 steel under effective cooling condition. *Neural Comput & Applic.* 31 : 2349–2370. <https://doi.org/10.1007/s00521-017-3192-4>
- [34] Perez M et al (2009) Microstructural evolution of martensitic 100Cr6 bearing steel during tempering: from thermoelectric power measurements to the prediction of dimensional changes. *Acta Mater* 57 : 3170–3181. <https://doi.org/10.1016/j.actamat.2009.03.024>
- [35] Marcin Barszcz et al (2017) Evaluation of tribological properties of selected engine oils during operation of the friction pairs of steel-on-steel, E3S Web of Conferences. 19 : 03027. <https://doi.org/10.1051/e3sconf/20171903027>
- [36] Senatore, A.; Risitano, G.; Scappaticci, L.; D'Andrea, D (2021) Investigation of the Tribological Properties of Different Textured Lead Bronze Coatings under Severe Load Conditions. *Lubricants*. 9 :34. <https://doi.org/10.3390/lubricants9040034>.
- [37] F. Schultheiss, D. Johansson, V. Bushlya, J. Zhou, K. Nilsson, and J.-E. Ståh (2017) Comparative study on the machinability of lead-free brass. *J. Clean. Prod* 149 : 366–377. <https://doi.org/10.1016/j.jclepro.2017.02.098>
- [38] P. García, S. Rivera, M. Palacios, and J. Belzunce (2010) Comparative study of the parameters influencing the machinability of leaded brasses. *Eng. Fail. Anal* 17: 771–776. <https://doi.org/10.1016/j.engfailanal.2009.08.012>
- [39] N. Gane (1981) The effect of lead on the friction and machining of brass. *Philos. Mag. A*, 43: 545–566. <https://doi.org/10.1080/01418618108240394>
- [40] Like Pan et al (2017) Temperature Effects on the Friction and Wear Behaviors of SiCp/A356 Composite against Semi metallic Materials. *Advances in Materials Science and Engineering*. 1824080 : 12. <https://doi.org/10.1155/2017/1824080>
- [41] I Gil (2016) Influence of the tool temperature increment on the coefficient of friction behavior on the deep drawing process of HSS. *IOP Conf. Series: Materials Science and Engineering* 159. <https://doi.org/10.1088/1757-899X/159/1/012019>
- [42] S.R. Pearson (2013) The effect of temperature on wear and friction of a high strength steel in fretting. *Wear* 303 :622–631. <https://doi.org/10.1016/j.wear.2013.03.048>
- [43] Merklein M, Zoeller F and Sturm V (2014) Experimental and numerical investigations on frictional behavior under consideration of varying tribological conditions. *Adv. Mater. Res* 966-967:270–8. <https://doi.org/10.4028/www.scientific.net/AMR.966-967.270>
- [44] Ferreira RO et al (2019) Characterization and evolution of the coefficient of friction during pin on disc tribotest: Comparison between C10200 Cu, AA6082-T6 Al and C36000 brass pins under varying normal loads. *Tribol Int.* 138 : 403–414. <https://doi.org/10.1016/j.triboint.2019.06.013>
- [45] Okonkwo PC, Kelly G, Rolfe BF, Pereira MP (2016) The effect of sliding speed on the wear of steel–tool steel pairs, *Tribol Int.* 97 : 218–227. <https://doi.org/10.1016/j.triboint.2016.01.030>
- [46] Seyf Eddine BM, Noura M (2019) A Comparative Study on the tribological behavior of SAE-AISI 1055 steel and brass (CuZn39Pb2) a pin on disc type of contact. *Defect Diffusion Forum*. 397 : 147–160.

<https://doi.org/10.4028/www.scientific.net/DDF.397.147>

- [47] Dalverny O, Caperaa S, Pantale O, Sattouf C (2002) Identification of constitutive laws and friction laws adapted to high strain rates. *J Phys IV* 12(PR11) : 275-281. <https://doi.org/10.1051/jp4:20020503>
- [48] Jamal Nasir Hussain Al Katib (2015) Investigation of Wear Behavior of 1060 and 1095 Steels using Regression Analysis. *Eng. &Tech. Journal.* 33 : 753-761. <https://www.iasj.net/iasj/article/101939>
- [49] Ming C et al (2018) Wear behavior of Al<sub>0.6</sub>CoCrFeNi high entropy alloys: effect of environments, *J Mater Res.* 3319 : 3310-3320. <https://doi.org/10.1557/jmr.2018.279>
- [50] Lyu Y, Wahlström J, Tu M, Olofsson U, Friction A (2018) Wear and emission tribometer study of non-asbestos organic pins sliding against AlSiC MMC Discs, *Tribol Ind* 40 : 274-282. <https://doi.org/10.24874/TI.2018.40.02.11>
- [51] Sivasankaran S (2019) Optimization on dry sliding wear behavior of yellow brass using face centered composite design, *AIMS Mater Sci.* 6 : 80-96. <https://doi.org/10.3934/mater.sci.2019.1.80>
- [52] Seyf Eddine BM et al (2020) An assessment of tribological characteristics under different operating condition, *Adv Mater Lett.* 11 : 2. <https://doi.org/10.5185/amlett.2020.021478>
- [53] MN Bachirbey et al (2021) A Comparative Study of Microstructure, Coefficient of Friction and Wear Rate of Alloy Ni-Cr-B-Si-CW, *Defect and Diffusion Forum.* 406 : 229-239. <https://doi.org/10.4028/www.scientific.net/DDF.406.229>
- [54] Mia, M., Dhar, N.R (2019) Prediction and optimization by using SVR, RSM and GA in hard turning of tempered AISI 1060 steel under effective cooling condition. *Neural Comput & Applic* 31 : 2349-2370. <https://doi.org/10.1007/s00521-017-3192-4>
- [55] M. Nurizinova, Sherzod Ramankulov, M. Skakov, (2022) Evaluation of advanced technology for the formation of research competence of physics students in the field of tribology 4: 136-152. <https://doi.org/10.32014/2022.2518-1483.177>